

SERI/TP-217-3269
UC Category: 60
DE88001118

Turbulence Loads on the Howden 26-m-Diameter Wind Turbine

P.H. Madsen
S.M. Hock
T.E. Hausfeld

November 1987

Prepared for the 7th ASME
Wind Energy Symposium
New Orleans, Louisiana
10-13 January, 1988

Prepared under Task No. WE721202

Solar Energy Research Institute

A Division of Midwest Research Institute

1617 Cole Boulevard
Golden, Colorado 80401-3393

Prepared for the
U.S. Department of Energy
Contract No. DE-AC02-83CH10093

NOTICE

This report was prepared as an account of work sponsored by the United States Government. Neither the United States nor the United States Department of Energy, nor any of their employees, nor any of their contractors, subcontractors, or their employees, makes any warranty, expressed or implied, or assumes any legal liability or responsibility for the accuracy, completeness or usefulness of any information, apparatus, product or process disclosed, or represents that its use would not infringe privately owned rights.

Printed in the United States of America
Available from:
National Technical Information Service
U.S. Department of Commerce
5285 Port Royal Road
Springfield, VA 22161

Price: Microfiche A01
Printed Copy A02

Codes are used for pricing all publications. The code is determined by the number of pages in the publication. Information pertaining to the pricing codes can be found in the current issue of the following publications, which are generally available in most libraries: *Energy Research Abstracts*, (*ERA*); *Government Reports Announcements and Index* (*GRA* and *I*); *Scientific and Technical Abstract Reports* (*STAR*); and publication, NTIS-PR-360 available from NTIS at the above address.

TURBULENCE LOADS ON THE HOWDEN 26-m-DIAMETER WIND TURBINE

Peter H. Madsen
 Susan M. Hock
 Tom E. Hausfeld

Solar Energy Research Institute
 Wind Research Branch
 Golden Colorado

ABSTRACT

Conducted in Palm Springs, Calif., a joint effort between SERI and James Howden and Company involved a comprehensive test program on the 330-kW Howden wind turbine with a three-bladed, fixed-hub rotor 26 m in diameter. Part of the measurement analysis is to quantify the turbulence loads during the steady-state production modes of operation. Assuming wind turbulence to be the cause of the random loads, the turbulence loads in terms of blade root-bending moments have been determined empirically by isolating the random or non-periodic part of the load signals using azimuthal averaging. Standard deviations as functions of wind speed, as well as power spectra of the loads, are presented.

The measured turbulence loads are compared to a recently developed model for turbulence loading of wind turbines. The model works in the frequency domain and uses the standard engineering representation of turbulence in terms of a coherence function and a wind-power spectrum at a fixed point in space. The turbulence load model accounts for the dominant mode of vibration for the load in question and is intended to be simple enough to be used for a preliminary load estimate for practical design purposes.

NOMENCLATURE

c_n	Coefficient
D	Separation
$E\{ \}$	Expected value
$F_n(\omega)$	Admittance functions
$H(\omega)$	System transfer function
l	Turbulence wave length
L	Turbulence length scale
m_o	Generalized mass
M	Bending moment
$p(\underline{r}, t)$	External load
q	Generalized modal load

Q	Shear force
r	Radius
R	Rotor radius
$R(\tau)$	Covariance function
$S(\omega)$	Power spectral density
t	Time
T	Modal amplitude
u	Longitudinal turbulence component
$U(\underline{r}, t)$	Longitudinal wind speed
U_o	Mean wind speed at hub height
v	In-plane turbulence component
x	Displacement

Greek symbols

α	Angle
β	Moment location coefficient
$\gamma(\tau)$	Blade mass density
δ	Logarithmic decrement
$\delta(\)$	Dirac's delta function
ζ	Damping ratio
θ	Angle
λ	Speed ratio
μ	Independent coherence parameter
$v(\tau)$	Wind load influence function
σ^2	Variance
τ	Time lag
$\phi(\tau)$	Mode shape function
$\chi(D, \omega)^2$	Coherence function
ω	Frequency

INTRODUCTION

During recent years, considerable attention has been given to the effects of atmospheric turbulence on the structural integrity of a wind turbine. Wind turbulence causes temporal and spatial variations in the wind speed across the rotor disc and manifests itself as a randomly varying aerodynamic load that is superposed on the periodic cyclic loads such as those caused by wind shear, tower shadow, yaw misalignment, and gravity. Thus, due to its random nature, turbulence acting on a horizontal-axis wind turbine (HAWT) in operation causes both large, but rarely occurring, peak loads as well as continuously appearing variable-amplitude fatigue loads. Theoretical studies (1,2) and experimental investigations (3) have clearly shown that the omission of turbulence loads will cause a significantly inadequate fatigue design.

The basic assumption for analyzing and modeling turbulence loads during stationary operation is that the random loads from turbulence are independent of the cyclic, deterministic loads. During data analysis, the periodic loads are found using azimuthal averaging (by binning the measured load signal in question with respect to the azimuthal angle of the rotor). The residual, when the averaged periodic signal is subtracted from the original, is then assumed to be the turbulence load. The analysis then proceeds with characterizing the statistical properties of the loads in terms of variance, spectra, distribution of peaks, etc., as functions of environmental and operational conditions.

When modeling the turbulence loads, three major problems exist: (1) to quantify the properties of the turbulence at a prospective site, (2) to translate the information to fluctuations in wind speed along the turbine blades, and (3) to go from wind fluctuations to aerodynamic loads and internal forces in a dynamically active structure.

Although not complete, a large data base exists in the field of atmospheric science on the properties of turbulence for various terrain characteristics and atmospheric conditions. The properties of the turbulence are usually expressed in a Eulerian fixed frame of reference in terms of spectral densities of the velocity components at a fixed point, and coherencies and phase spectra to characterize the statistical correlation between velocities at two points. An engineering approximation that uses an exponential coherence function and an identically zero phase spectrum has often been used in the dynamic analysis of wind excitation of large civil-engineering structures (4).

The effect of moving through the turbulence in a vertical plane perpendicular to the wind direction must be represented when modeling the local wind fluctuations along the blade. The rapid motion of the blade through a slowly varying turbulence causes a redistribution of the wind turbulence spectrum to higher frequencies (5). There is also a theoretical explanation (6), where a model of the spectrum of longitudinal turbulence as seen by a rotating blade was developed assuming isotropic, incompressible turbulence and a Gaussian fixed-point spectrum. Similar models were presented (7,8) using the more realistic Von Karman model of isotropic turbulence.

There are two basically different approaches to calculating turbulence loads: (1) a time-integration approach, where the turbulent wind field across the rotor disc is simulated and used as input to the

aerodynamic and structural model; and (2) a spectral-analysis approach, which is a statistical frequency-domain approach. The advantage of the spectral-analysis method is computational efficiency at the cost of linear aerodynamic and structural models. Most models (1,2,9) are based on the isotropic Von Karman turbulence model and cannot fully make use of the available experimentally determined turbulence information. In contrast, the engineering representation in terms of a fixed-point spectrum and coherence function was used in a recent model (1). This model was based on the periodicity of the coherence function, as it applies to a rotating blade, to obtain a series solution for turbulence spectra at or between discrete points.

The present model assumes axisymmetric turbulence but otherwise uses experimentally determined turbulence properties. Like the model described in (9), it applies the expansion technique to obtain a series solution for the load spectrum. However, instead of expanding the total wind field, the generalized modal load is expanded in the blade azimuth angle such that additional terms can be easily included. The model is not intended for the final verification of a complex design but rather for giving preliminary load values for the beginning of the design cycle. The model requires only a few basic characteristics of the turbine, assumes linear aerodynamics, and approximates the basic dynamic properties of the blade by single-degree-of-freedom (SDOF) systems, each corresponding to a generalized load. The model complements that of (10), which is a simple model for rotor loads from turbulence but has a considerably simpler turbulence load model.

THE HOWDEN HAWT TEST

As part of the SERI/DOE Cooperative Field Test Program, a comprehensive measurement program has been carried out on a 330-kW Howden HAWT near Palm Springs, Calif. The measured data include wind data to characterize the full wind field in front of the turbine, and wind-turbine data to map the operational conditions and internal structural loads.

The wind turbine, manufactured by the British company of James Howden and Company, Ltd., is owned by Southern California Edison and is located at their Wind Energy Test Center in the northwest corner of the Coachella Valley, 10 km north of Palm Springs. The valley floor is a very flat desert with occasional scrub extending 3 km to the west, where the Whitewater hills rise approximately 300 m. The wind is primarily thermally driven, with a strong diurnal cycle; during practically all energy production, the wind direction is due west. The measurements for this paper were taken during September and October 1986, at the end of the windy season.

The wind turbine has a three-bladed, fixed-pitch rotor with a diameter of 26 m and a nominal rotation speed of 42 rpm. An up-wind machine with active yaw, it is rated at 330 kW at 14.5 m/s (at hub height, which is 24.1 m). Cut-in and cut-out wind speeds are 6 m/s and 28 m/s, respectively. The structure is basically comprised of an untapered tubular tower, a steel bed-plate, and a wood-epoxy rotor with a solidity of approximately 8 percent. The blade's fundamental frequencies are estimated to be 1.68 Hz and 4.06 Hz in the flapwise and chordwise directions, respectively. The blade's mass is 855 kg, with a mass density of 36.5 kg/m³ at 70 percent radius. Power control and overspeed protection are provided by drag-control using 2-m-long, variable-pitch tips. The turbine description

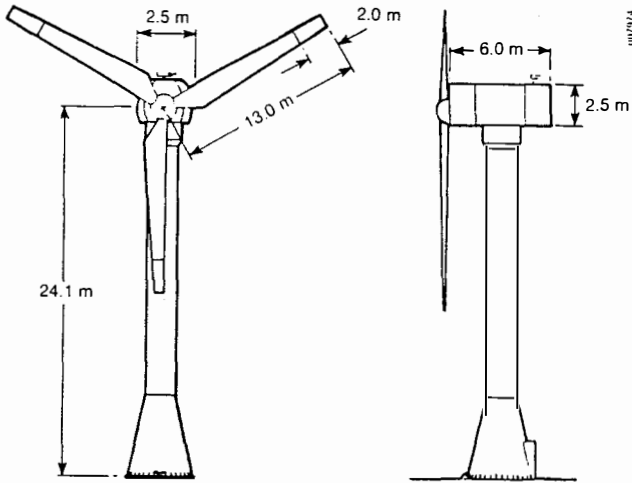


Fig. 1. The Howden 26-m-diameter, 330-kW wind turbine

and some results from Howden's analysis of the recorded data are given in (11). The turbine is shown in Fig. 1.

A total of 44 channels were recorded on a Honeywell 101 14-channel magnetic tape recorder in multiplexed form after having passed through 10-Hz low-pass active 6-pole filters. Of the 44 channels, 31 were used to obtain atmospheric data. Most wind speeds were recorded from a vertical-plane array of 3-axis UVW Gill propeller anemometers located 21 m west of the turbine. The wind speed at hub height was used as the reference for this study. Of the structural measurements, the bending moments at the 1.5-m radius in the flapwise and chordwise directions, and the flapwise bending moment at the 8.25-m radius, were used. The recorded analog signals were digitized at SERI using the NEFF 720 system with a sample rate of 41.67 Hz.

A number of digitized bending-moment time series of 10 min were selected at various wind speeds and averaged against the azimuth angle using a bin width of 10 degrees for the rotor azimuth-angle signal. A sixth-order Fourier series was fitted to the calculated average periodic signal. The series was then used to extract the periodic part from the total signal to get the turbulence-induced part. The residual signal was block-averaged to an effective sample rate of 20.83 Hz, and statistics and power spectra were calculated.

Preliminary results on the azimuth-averaged wind-turbine signals as a function of wind condition can be found in (12).

MODELING THE WIND TURBULENCE

Unless deeply in stall, the primary effect of wind fluctuation is the change in the angle of attack of the relative wind with respect to the blade profile. Ignoring induced velocities, the angle of attack can be written as

$$\alpha = \arctan \left\{ \frac{U_0 + u}{\omega_R r + v} \right\} - \theta_0 \quad , \quad (1)$$

where U_0 is the mean wind speed, u and v are the longitudinal and in-plane wind fluctuations, respectively, r is the radius, ω_R is the rotation frequency in rad/s, and θ_0 is the pitch angle. Since u and v are generally small compared to U_0 and $\omega_R r$, the following perturbation expression for changes in α from wind fluctua-

tions is obtained as the first-order term in a Taylor expansion:

$$\Delta\alpha = \frac{\lambda^2}{1+\lambda^2} \left(\lambda \frac{u}{U_0} - \frac{v}{U_0} \right) \quad . \quad (2)$$

The speed ratio λ is given by

$$\lambda = \omega_R r / U_0 \quad . \quad (3)$$

For the highest loaded outer part of the blade, λ is typically of the order of 3-5; since v/U_0 is 75 percent or less of u/U_0 in magnitude (13), the dynamic wind loads from turbulence are primarily caused by the fluctuations u in the mean wind direction. The wind field acting on the turbine rotor will therefore be described as

$$U(\underline{r}, t) = U_0(\underline{r}) + u(\underline{r}, t) \quad . \quad (4)$$

$U_0(\underline{r})$ is the 10-min average wind speed, which varies with height and depends on the terrain roughness, atmospheric stability, and local topography. The turbulent longitudinal fluctuation u will be modeled as a homogeneous and stationary random field across the rotor disc. The field has a zero mean and a cross covariance, which may be calculated from the cross-spectrum as

$$\begin{aligned} R_u(\underline{r}_1 - \underline{r}_2, \tau) &= E \{ u(\underline{r}_1, t + \tau) u(\underline{r}_2, t) \} \\ &= \int_{-\infty}^{\infty} S_u(\underline{r}_1 - \underline{r}_2, \omega) e^{i\omega\tau} d\omega \quad . \quad (5) \end{aligned}$$

The site is located in a very flat and smooth desert area, with hills and mountains beginning at a distance of 3 km. The wind is thermally driven with due west as the prevailing wind direction. The extreme thermal radiation makes it questionable whether neutral stratification of the atmosphere is found across the rotor disc, even for higher wind speeds. This and the proximity of the mountains invalidates the usual assumptions for turbulence intensity, length scale, and coherence decay factors for a homogeneous terrain and neutral atmosphere.

The turbulence properties used in this paper are based on the analysis of wind data from the vertical array 21 m due west of the wind turbine. Data from seven 3-axis propeller anemometers were used; one was centered in the array at hub height, and the other six were evenly spaced around the first at a radius of 13 m (corresponding to the blade length).

A one-sided power spectrum (i.e., defined for positive frequencies only with a value of twice the standard two-sided power spectrum) with the analytical form (14)

$$\frac{\omega S_u(\omega)}{\sigma_u^2} = \frac{\omega L / U_0}{(1 + 1.5 \omega L / U_0)^{5/3}} \quad , \quad (6)$$

was fitted to the calculated power spectra from low-, medium-, and high-wind-speed data series measured by the hub-height anemometer. L is the turbulence length scale. The data series were selected as representing neutral or slightly unstable atmospheric conditions. Spectra of signals from anemometers at other heights showed only minor deviations, and equation (6), with parameters $L = 192$ m and $\sigma_u / U_0 = 0.15$, is assumed to be representative for the fixed-point spectrum of the longitudinal turbulence component for all points in the rotor disc.

Coherence functions and phase spectra were estimated with 135 statistical degrees of freedom between the hub-height anemometer and the anemometers in the 13-m-radius ring and between anemometers symmetrical with respect to the hub. All phase spectra showed a random scatter around zero, and all coherence functions showed a reasonable agreement when plotted with

$$\mu = \{(\omega D/U_0)^2 + (D/L)^2\}^{1/2} \quad (7)$$

as the independent parameter. D is the separation between anemometers. The cross spectrum, between the turbulent longitudinal wind fluctuations at points on a plane perpendicular to the mean wind direction, is proposed to have the form

$$S_u(\underline{r}_1 - \underline{r}_2, \omega) = S_u(\omega) \chi(D, \omega), \quad (8)$$

with $S_u(\omega)$ given in equation (6) and

$$\chi(D, \omega) = \exp[-2.07 \mu^2 / (0.66 + \mu)]. \quad (9)$$

The parameters in equation (9) were estimated using a least-square fit of χ^2 to the measured coherencies. The proposed square root of the coherence function in equation (9) only deviates from the simple exponential model of Davenport (15) for small values of ω . A significant difference is that, unlike the Davenport model and in agreement with the Von Karman isotropic turbulence model, the model discussed in (9) does not predict a coherence of one at zero frequency and a nonzero separation. This becomes extremely important for correctly predicting the peaks at multiples of the rotation frequency at rotationally sampled turbulence spectra (16).

LOAD AND RESPONSE

We shall assume that all turbulence-induced internal forces needed for the structural design are caused by turbulence loads on the blades only. Furthermore, we shall assume that the considered blade response is associated with one degree of freedom or one mode of vibration. To set up the equations for the blade loading and response, consider a frame of reference that rotates with the blades. Hence, the blade displacement can be expressed by

$$x(r, t) = \phi(r) T(t), \quad (10)$$

where $\phi(r)$ is the mode shape function and $T(t)$ is the modal amplitude. In terms of $T(t)$, the equation of motion is

$$\ddot{T} + 2\omega_0 \zeta_0 \dot{T} + \omega_0^2 T = q/m_0 = 1/m_0 \int_R p(\underline{r}, t) \phi(r) dr, \quad (11)$$

in which ω_0 is the modal frequency in rad/s, ζ_0 is the structural damping ratio, $p(\underline{r}, t)$ is the external loading, and m_0 is the generalized mass, given by

$$m_0 = \int_R \gamma(r) \phi(r)^2 dr, \quad (12)$$

where R is the blade length and $\gamma(r)$ is the mass density along the blade.

Assuming linearity between the turbulent wind fluctuations $u(\underline{r}, t)$, the load $p(\underline{r}, t)$ can be expressed as

$$p(\underline{r}, t) = v(r) [u(\underline{r}, t) - x_f(r, t)], \quad (13)$$

in which $x_f(r, t)$ is the flapwise displacement and $v(r)$ is the wind load influence function. From equation (13), the modal load becomes

$$q = q^e(\alpha, t) - 2\omega_0 \zeta_a \dot{T}, \quad (14)$$

where $q^e(\alpha, t)$ is the effective generalized load and ζ_a is the aerodynamic damping ratio for a flapwise modal vibration

$$\zeta_a = \frac{1}{2\omega_0 m_0} \int_R v(r) \phi(r)^2 dr \quad (15)$$

and

$$q^e(\alpha, t) = \int_R v(r) u(r, \alpha, t) \phi(r) dr. \quad (16)$$

Note that $q^e(\alpha, t)$ is a function of the blade azimuth angle α . Clearly, at a given instant t , q^e is periodic in α and can be expanded in a Fourier series. Thus,

$$q^e(\alpha, t) = q_0(t) + \sum_{n=1}^{\infty} [q_n^c(t) \cos n\alpha + q_n^s(t) \sin n\alpha], \quad (17)$$

with the coefficients given by

$$\begin{aligned} q_0(t) &= \frac{1}{2\pi} \int_0^{2\pi} \int_0^R v(r) u(r, \alpha, t) \phi(r) d\alpha dr \\ &= \frac{1}{2\pi} \int_{\text{disc}} \frac{v(r)\phi(r)}{r} u(r, \alpha, t) dA \end{aligned} \quad (18)$$

and

$$\begin{cases} q_n^c(t) \\ q_n^s(t) \end{cases} = \frac{1}{\pi} \int_{\text{disc}} \frac{v(r)\phi(r)}{r} u(r, \alpha, t) \begin{cases} \cos n\alpha \\ \sin n\alpha \end{cases} dA. \quad (19)$$

For periodic loading and stationary random vibration, the equation of motion (11) is conveniently solved in the frequency domain, where the Fourier transforms of $T(t)$ and q^e relate as

$$\tilde{T}(\omega) = \frac{H(\omega)}{m_0 \omega_0^2} \tilde{q}^e(\omega), \quad (20)$$

where ω is the frequency in rad/s and $H(\omega)$ is the modal transfer function

$$H(\omega) = [1 - (\frac{\omega}{\omega_0})^2 + i \frac{\delta}{\pi} \frac{\omega}{\omega_0}]^{-1}. \quad (21)$$

In equation (21), use is made of the logarithmic decrement of the damping $\delta \approx 2\pi(\zeta_0 + \zeta_a)$. Note that for $\omega \ll \omega_0$ or when δ is large, $H(\omega)$ can be conservatively set to one.

By applying an inverse Fourier transform to $\tilde{T}(\omega)$, the modal amplitude and hence the blade displacement from equation (10) is obtained as a function of time. In principle, the internal forces, such as bending moments and shear forces, can be obtained from differentiating the displacements; however, using an estimated mode shape function may produce significantly inaccurate results. A more robust method consists of applying fictitious static external loads that would cause the blade to deform in its assumed mode shape (17). This fictitious inertia-type loading is given by

$$p^*(r) = \gamma(r) \phi(r) \omega_0^2 T, \quad (22)$$

from which blade root moments M and root shear forces Q are calculated as

$$M = T \int_0^R \omega_0^2 r \gamma(r) \phi(r) dr \quad (23)$$

and

$$Q = T \int_0^R \omega_0^2 \gamma(r) \phi(r) dr . \quad (24)$$

Since the turbulent wind field is modeled as a random field, we shall characterize the modal amplitudes and hence the internal forces by mean values and covariance functions. From equation (20) and the definitions of mean and covariance (18), the mean value of T is

$$E\{T\} = 0 = \frac{1}{m_0 \omega_0^2} \int_R E\{p(r,t)\} \phi(r) dr \quad (25)$$

and the covariance is

$$R_T(\tau) = \frac{1}{(m_0 \omega_0^2)^2} \int_{-\infty}^{\infty} |H(\omega)|^2 S_q(\omega) e^{i\omega\tau} d\omega, \quad (26)$$

where the spectrum of the generalized load is given by

$$S_q(\omega) = \frac{1}{2\pi} \int_{-\infty}^{\infty} E\{q e^{i\omega(t+\tau)}, t+\tau\} q e^{i\omega t} dt \quad (27)$$

$$= \frac{1}{2\pi} \int_{-\infty}^{\infty} R_q(\tau) e^{-i\omega\tau} d\tau .$$

Introducing the expansion in equation (17) in calculating $R_q(\tau)$, we find that $R_q(\tau)$ is composed of the covariances of the expansion coefficients. Assuming that the turbulence field is axisymmetric with respect to the mean wind direction, the symmetry has, as a consequence (16),

$$R_q^n(\tau) = E\{q_n^c(t+\tau) q_n^c(t)\} = E\{q_n^s(t+\tau) q_n^s(t)\}$$

$$= c_n \int_0^R \int_0^R \int_0^{2\pi} v(r_1) v(r_2) \phi(r_1) \phi(r_2) \times R_u(r_1, r_2, \tau) \cos n\alpha \, d\alpha \, dr_1 / dr_2 , \quad (28)$$

where R_u is the covariance function of the turbulent wind field (5), $\underline{r} = (r, \alpha)$, $\alpha = \alpha_1 - \alpha_2$ and

$$c_n = \begin{cases} \frac{1}{2\pi} & \text{for } n=0 \\ \frac{1}{\pi} & \text{for } n>0 \end{cases} . \quad (29)$$

Covariances between terms of different order and between cosine and sine terms are identically zero.

Hence, R_q is given by the series

$$R_q(\alpha, \tau) = R_q^0(\omega) + \sum_{n=1}^{\infty} R_q^n(\tau) \cos n\alpha . \quad (30)$$

While transforming equation (30) to the frequency domain to give the generalized load spectrum, it should be noted that for a rotating blade

$$\alpha = \omega_R \tau , \quad (31)$$

where ω_R is the rotation frequency in rad/s. Since multiplication in the time domain corresponds to convolution in the frequency domain, and

$$\frac{1}{2\pi} \int_{-\infty}^{\infty} \cos(n\omega_R \tau) e^{-i\omega\tau} d\tau = 1/2 [\delta(\omega - n\omega_R) + \delta(\omega + n\omega_R)] , \quad (32)$$

in which $\delta(\)$ is the Dirac delta function, we get

$$S_q(\omega) = S_q^0(\omega) + 1/2 \sum_{n=1}^{\infty} [S_q^n(\omega - n\omega_R) + S_q^n(\omega + n\omega_R)] . \quad (33)$$

Using the the wind-turbulence cross spectrum in equation (8), the component spectra in equation (33) are given by

$$S_q^n(\omega) = S_u(\omega) \left[\int_R v(r) \phi(r) dr \right]^2 F_n(\omega) c_n , \quad (34)$$

in which F_n acts as an aerodynamic admittance function and has the form

$$F_n(\omega) = \left[\int_R v(r) \phi(r) dr \right]^{-2} \times \int_0^{2\pi} \int_0^R \int_0^R v(r_1) v(r_2) \phi(r_1) \phi(r_2) \times \chi(\underline{r}_1 - \underline{r}_2, \omega) \, dr_1 dr_2 d\alpha . \quad (35)$$

TURBULENCE BLADE LOADS FOR DESIGN

Based on the presented theory, we shall now develop a simple expression for the turbulence blade loads in the flapwise and the chordwise directions, based on additional simplifying assumptions. Assume first that the out-of-plane aerodynamic load distribution is proportional to the radius, whereas the in-plane load distribution is constant with the radius. This is a reasonable assumption, as shown in Fig. 2, where the aerodynamic load distributions are in both directions at two different wind speeds. The distributions were calculated using SERI's blade element code, PROPPC. Secondly, assume that the flapwise mode shape can be given as the simplest polynomial that satisfies the static and kinematic boundary conditions of a fixed-free cantilevered blade. Turbulence loading in the chordwise direction is of lesser importance and, since some flexibility in the drive train is expected, the in-plane mode shape is simply assumed to be linear in the radius. The mass distribution of a blade is usually highly nonuniform, with mass concentrated at the hub. The mass density does not vary much for the outer half of the blade, which experiences the largest amplitude motion; we shall therefore assume a constant mass density corresponding to the density at 70 percent radius. Finally, the aerodynamic damping in the chordwise direction is assumed to be zero. These assumptions, and the resulting generalized mass and the flapwise aerodynamic damping, are summarized in Table 1.

Using the mode shapes and the aerodynamic load distributions, $F_n(\omega)$ can be calculated numerically from equation (35). The modal admittance functions are functions of one parameter, namely

$$\mu^* = \{(\omega R / U_0)^2 + (R/L)^2\}^{1/2} , \quad (36)$$

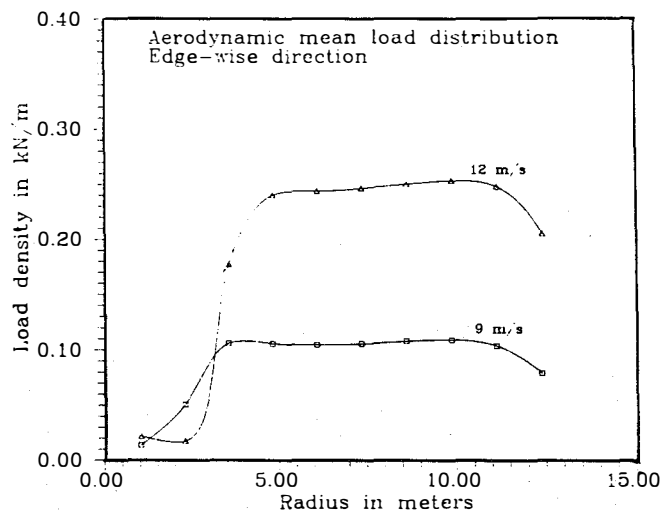
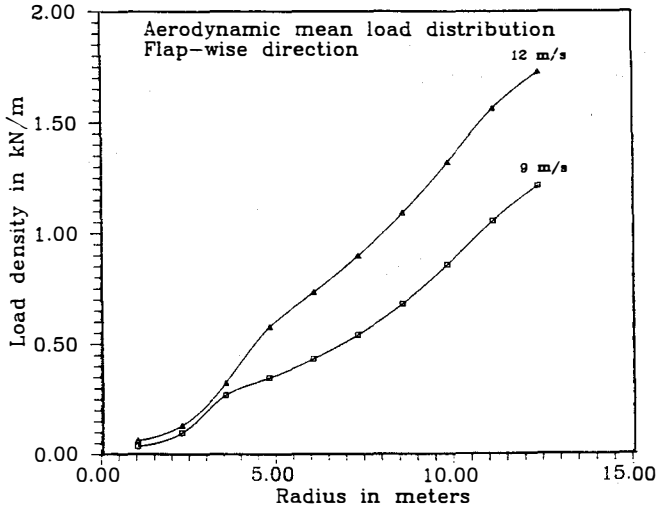


Fig. 2. Calculated aerodynamic load distributions on the Howden machine using PROPPC

and can thus be tabulated once and for all. The modal admittance functions for flapwise and chordwise bending are shown in Fig. 3 for ascending orders $n=0,1,2,3$ (the top curve represents the 0th order and the bottom curve represents the 3rd order). These functions are also tabulated in the appendix.

Note that the admittance functions act as filters, selecting a band of frequencies in the turbulence spectrum and hence a band of eddy sizes. In terms of turbulence wavelength, which for frozen turbulence is defined as

$$l = U_0/\omega \approx R/\mu^* \quad (37)$$

we can see that the generalized load component $q_0(t)$ is caused primarily by turbulence with wavelengths greater than the rotor diameter. The component that causes a load variation that is periodic with the azimuth angle comes from turbulence with wavelengths centered around the rotor diameter. The load variation that is periodic with twice the azimuth angle comes from turbulence with wavelengths of the order of the blade length. The load variation with three times the azimuth are from

Table 1. System Description

Flapwise Bending	Chordwise Bending
$v(r): v_0 r/R$	v_0
$\phi(r): \phi_0 [(\frac{r}{R})^4 - 4(\frac{r}{R})^3 + 6(\frac{r}{R})^2]$	$\phi_0 r/R$
$\gamma(r): \gamma_0 = \gamma$ (70% radius)	$\gamma_0 = \gamma$ (70% radius)
$m_0: 2.311 \gamma_0 \phi_0^2 R$	$0.333 \gamma_0 \phi_0^2 R$
$\zeta_a: 0.927 v_0 / (\gamma_0 \omega_0)$	0

turbulence with wavelengths of the order of 2/3 of the blade length. At high values of u^* and hence small wavelengths, the admittance functions coincide and decrease as μ^{*-2} . The modal admittance functions for flapwise and chordwise bending are rather close in spite of significant differences in mode shape and aerodynamic load distribution. This means that the results in terms of the turbulence load power spectra must be rather insensitive to the representation of mode shape and aerodynamic load distribution.

Using the fictitious external load from equation (22) to calculate the blade bending moment at radius a , we get

$$M(a) = B \omega_0^2 \gamma_0 \phi_0 R^2 T \quad (38)$$

in which B is given by

$$B = \int_{a/R}^1 (y-a/R) (y^4 - 4y^3 + 6y^2) dy \quad [\text{flapwise bending}]$$

$$= 0.867 + 1.2(a/R) + 0.5(a/R)^4 - 0.2(a/R)^5 + 0.033(a/r)^6 \quad (39)$$

and

$$B = \int_{a/R}^1 (y-a/R) y dy \quad [\text{chordwise bending}]$$

$$= 0.333 - 0.167(a/R)^2 - 0.5(a/R) \quad (40)$$

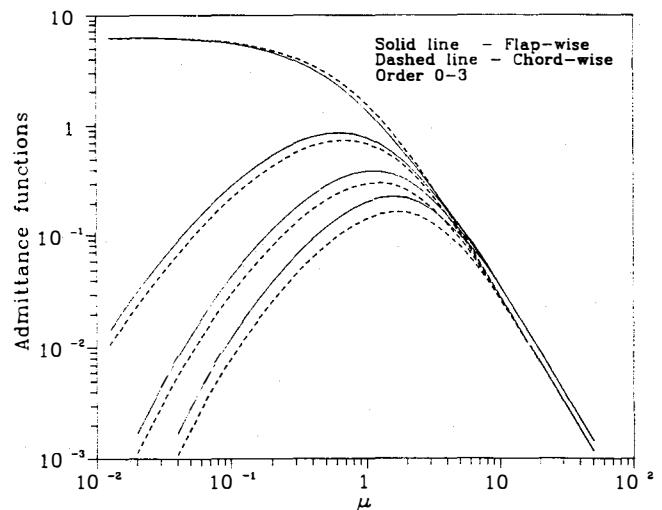


Fig. 3. Modal admittance functions

The covariance, and hence the power spectrum, of the modal amplitude T is defined in equation (26). Using the expansion of $S_u(\omega)$ from equations (33) and (34), the power spectrum of the bending moment, defined from $-\infty$ to $+\infty$, becomes

$$S_M(\omega) = [0.375 \beta v_o R^2]^2 |H(\omega)|^2 \sum_{n=0}^{\infty} c_n [S_u(\omega - n\omega_R) F_n(\omega - n\omega_R) + S_u(\omega + n\omega_R) F_n(\omega + n\omega_R)] \quad (41)$$

for flapwise bending and

$$S_M(\omega) = [1.5 \beta v_o R^2]^2 |H(\omega)|^2 \sum_{n=0}^{\infty} c_n [S_u(\omega - n\omega_R) F_n(\omega - n\omega_R) + S_u(\omega + n\omega_R) F_n(\omega + n\omega_R)] \quad (42)$$

for chordwise bending. The variance of the turbulence-induced blade moments are found by integrating the spectra with respect to frequency from $-\infty$ to $+\infty$.

Note that the information needed to obtain an estimate of the bending moments due to turbulence is limited to (1) an estimate of the modal frequency ω_0 and the modal structural damping ratio ζ_0 , (2) a characteristic mass density for the blade, and (3) an estimate of the aerodynamic load as a function of the wind speed. For a fixed-pitch machine, the last estimate can be derived from the rotor thrust and torque. Otherwise, an aerodynamic code, such as a blade element code, must be used.

COMPARISON BETWEEN PREDICTED AND MEASURED BLADE RESPONSE

A number of 10-min time series containing blade bending moments have been selected so that the operational wind-speed range is reasonably represented. As described earlier, the periodic part has been removed and the standard deviation and power spectrum of the residual have been calculated.

The structural data for the model were taken from (11), and the modal frequencies were set to 10.55 rad/s and 20 rad/s for flapwise and chordwise bending, respectively. The characteristic blade mass density is chosen as 36.5 kg/m. The mean flap-bending moment at the 1.5-m radius given in (11) grows linearly with the mean wind speed with a slope of 5 kNm/(m/s), from which $v_o = 0.108$ kNs/m. Using the power curve for wind speeds less than that rated, and using an efficiency of 0.95, the in-plane aerodynamic load density is estimated to be 0.035 kNs/m. The aerodynamic damping is calculated to be $\zeta_a = 0.11$ for the flapwise vibration, and a structural damping ratio of 0.02 is assumed for the edgewise motion.

The standard deviations of the turbulence flap-bending moments, which are proportional to the standard deviation of the turbulence fluctuations u , are shown in Fig. 4 as a function of wind speed. The model predictions (the solid line in the figure) are based on a turbulence intensity $\sigma_u/U_o = 0.15$, and the data points are scaled from the actual turbulence intensity to 0.15. The series solution for the spectra was truncated after $n=6$. The agreement is rather good, both at the 1.5-m and 8.25-m radii, which supports the assumption that the vibrational pattern is dominated by a single mode.

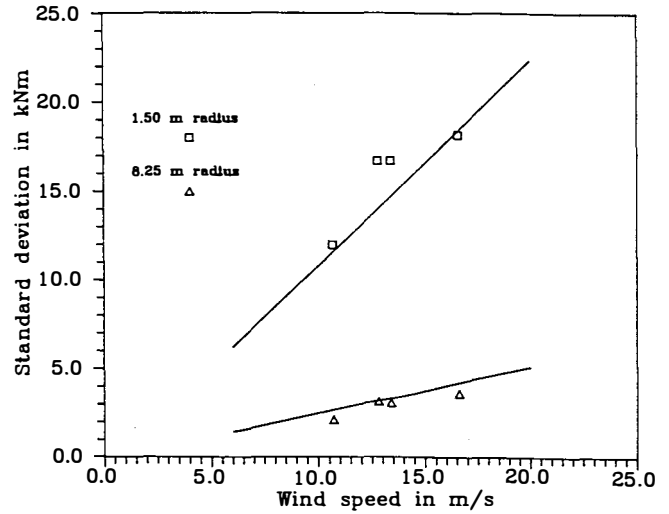


Fig. 4. Flap-bending moment as a function of wind speed

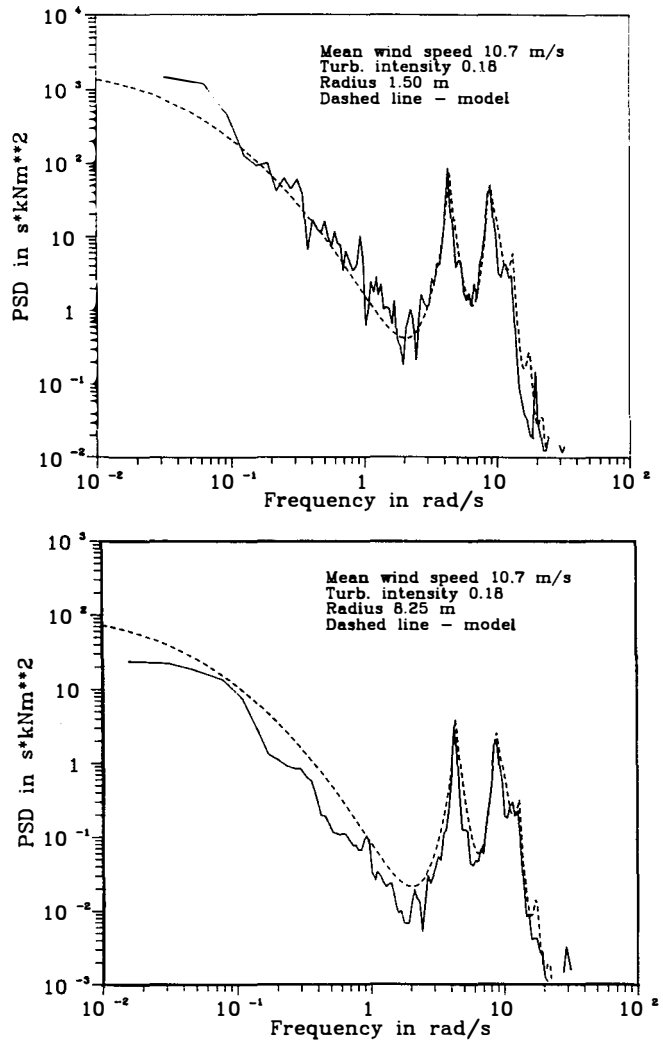


Fig. 5. Power spectra of flap-bending moments at a wind speed of 10.7 m/s

Fig. 5 shows the one-sided power spectra of the flap-bending moments at the 1.5-m and 8.25-m radii at a wind speed of 10.7 m/s. The experimentally determined

spectra are calculated by dividing the data series into three segments and averaging the resulting spectra. The number of points in the spectrum is reduced from 1024 to 200 using logarithmic averaging. The wind speed is below the rated wind speed, and the turbine operates as a fixed-pitch machine with an inactive pitch-control mechanism. The model predictions are shown in Fig. 5 with a dashed line. Note that the rotational sampling causes distinct peaks at one and two times the rotor speed, while peaks at three times the rotor speed and higher are hardly discernible. The agreement is better for the moment near the root than at the 8.25-m radius. Near the tip, however, deviations between the actual and assumed aerodynamic load distribution have more influence on the bending moment.

Fig. 6 shows the experimental and theoretical power spectra of flap-bending moments at a wind speed above the rated wind speed. The agreement is still fair, although discrepancies are noted particularly at low frequencies. This is because the bandwidth of the active pitch control system acts to remove low-frequency variations in the power output. The aerodynamic load distribution is thus varied actively near the tips. As could be expected, the differences between data and the model, which does not account for the variable pitch, are largest at the 8.25-m radius.

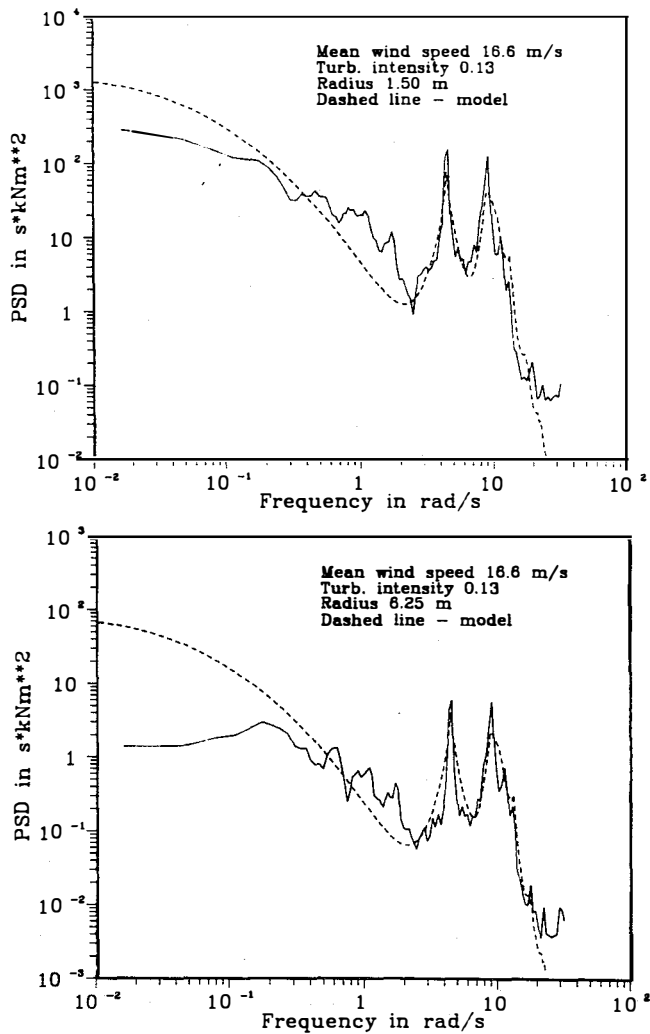


Fig. 6. Power spectra of flap-bending moments at a wind speed of 16.6 m/s

Finally, Fig. 7 shows the one-sided power spectral density of the edgewise bending moment at the 1.5-m radius and a wind speed of 10.7 m/s (i.e., inactive pitch control). Overall agreement is quite good, although the experimentally determined spectrum is somewhat irregular. Note that the turbulence loading in the edgewise direction is an order of magnitude smaller than in the flapwise direction. Again, the response seems to be dominated by a single mode of vibration. However, the amplification at the resonance is overestimated, possibly because of an unaccounted damping in the drive train. Above the rated wind speed, the pitch control strongly affects the edgewise response and the model is a priori considered insufficient.

CLOSING DISCUSSION

As can be seen from the spectra, the Howden 26-m wind turbine shows a relatively benign behavior with respect to turbulence loads. The choice of power regulation causes the flapping resonance to be aerodynamically damped above the rated wind speed. Unfortunately, the fundamental flap frequency is close to two times the rotation frequency. As a result, the blade bending spectra are dominated by peaks at one and two times the rotation frequency. The agreement between the experimental and theoretical bending-moment spectra is good, which for this rather stiff and heavy turbine type justifies the assumptions of a single dominant mode and linear aerodynamics in the context of the model's simplicity.

The flapwise bending-moment spectra drops rapidly for frequencies higher than two or three times the rotation frequency, whereas the higher edgewise resonance makes the fourth and fifth peaks visible. It is expected that the series for the bending moment spectra, shown in equations (41) and (42), can generally be truncated after $n=6$. This, and the fact that no time and computer-storage-demanding digital Fourier transforms are made, makes the model very convenient and provides instant answers using a microcomputer. The model has the advantage of not assuming isotropic turbulence and a certain spectral shape. With this additional generality, data of turbulence dependency on terrain effects and atmospheric stability can be used directly.

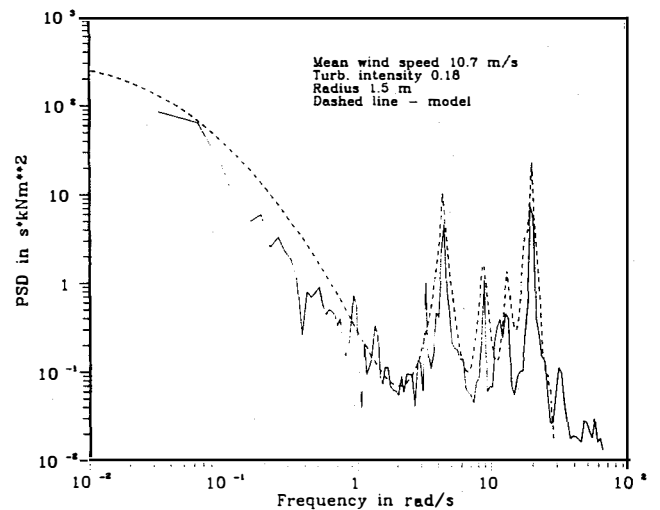


Fig. 7. Power spectrum of the edgewise bending moment at a wind speed of 10.7 m/s

The model can be extended to rotor loads (16) by adding the blade contributions with the correct phase. For a perfectly balanced rotor with three blades, the spectra of the rotor loads, thrust, torque, tilt, and yaw moment will show peaks at three times the rotation frequency (and multiples thereof) in addition to the filtered background turbulence.

The model cannot handle the dynamic effects of pitch regulation without further complication. This causes the model predictions, especially for the chord-wise bending, to be conservative for wind speeds above the rated power level or when the pitch control becomes active. In addition, the model will be inaccurate for very flexible turbine types, where two or more blade modes become equally excited. In spite of the limitations, the simplicity and the demonstrated agreement between model and reality make the model a good tool to estimate preliminary turbulence loads for the first round in the design process.

CONCLUSIONS

The effect of wind turbulence on the blade-bending moments of the Howden 26-m wind turbine has been investigated. The standard deviation of the flap-bending moments increases almost linearly with wind speed. The power spectra of the flap-bending moments are dominated by peaks at one and two times the rotation speed, above which the energy content in the spectra drops rapidly. The fundamental flap frequency almost coincides with the second peak, which causes a considerable high-frequency content in the flapwise response.

A newly developed model for turbulence blade loads is presented and compared to measured data. The model accounts for only one mode of vibration and uses only a few parameters to characterize the turbine blade. The model agrees very well with the data, especially below the rated wind speed, where the turbine operates as a fixed-pitch machine. Part of the reason for the good agreement is that the model uses experimentally determined wind spectra and coherence functions as opposed to the common assumption of isotropic turbulence.

ACKNOWLEDGEMENTS

This work was sponsored by the U.S. Department of Energy under Contract No. DE-AC02-83CH10093.

REFERENCES

1. Madsen, P.H. and Frandsen, S., "Wind-Induced Failure of Wind Turbines," Proceedings of Design Against Wind-Induced Failure, 12-13 January, 1984, Bristol, UK, Engineering Structures, 1984.
2. Garrad, A.D. and Hassan, U., "Taking the Guesswork out of Wind Turbine Design," Proceedings of the Wind Energy Expo '86 and National Conference, Sept. 1-3, 1986, Cambridge, Mass., American Wind Energy Association, pp. 164-176.
3. Stoltze, C.L., "An Evaluation of Turbulence-Induced Fatigue Loads Sustained by a Large Scale, Compliant HAWT Rotor," Proceedings of the Sixth ASME Wind Energy Symposium, Feb. 15-18, 1987, Dallas, Texas, American Society of Mechanical Engineers, pp. 1-8.
4. Davenport, A.G., "Gust Loading Factors," Journal of the Structural Division, Proc. ASCE, No. ST3, June 1967, pp. 11-34.
5. Connell, J.R., "Turbulence Spectrum Observed by a Fast-Rotating Wind Turbine Blade," PNL-3426, 1980, Battelle Pacific Northwest Laboratory, Richland, Wash.
6. Rosenbrock, H.H., "Vibration and Stability Problems in Large Turbines Having Hinged Blades," C/T 113, 1955, ERA Technology Ltd., Leatherhead, Surrey.
7. Kristensen, L. and Frandsen, S., "Model for Power Spectra of the Blade of a Wind Turbine Measured from the Moving Frame of Reference," Journal of Wind Engineering and Industrial Aerodynamics, Vol. 10, 1982, pp. 249-262.
8. Connell, J.R., "The Spectrum of Wind Speed Fluctuations Encountered by a Rotating Blade of a Wind Energy Conversion System," Solar Energy, Vol. 29, No. 5, 1982, pp. 363-375.
9. Holley, W.E., Thresher, R.W., and Lin, S.-R., "Atmospheric Turbulence Inputs for Horizontal Axis Wind Turbines," Proceedings of the European Wind Energy Conference, 22-26 October, 1984, Hamburg, West Germany, H.S. Stephens and Associates, pp. 443-452.
10. Madsen, P.H., "Simplified Rotor Loads from Wind Turbulence," Proceedings of the European Wind Energy Conference, 22-26 October, 1984, Hamburg, West Germany, H.S. Stephens and Associates.
11. Redmond, I., Anderson, C.G., and Jamieson, P., "Dynamic Response of a 330 kW Horizontal Axis Wind Turbine Generator," Draft report, June 1987, James Howden & Co., Glasgow, Scotland.
12. Hausfeld, T., Hock, S., and Hampson, G., "Preliminary Field Test Results for the Howden Wind Turbine," presented at the Windpower '87 conference, San Francisco, Calif., October 5-8, 1987.
13. Panofsky, H.A. and Dutton, J.A., Atmospheric Turbulence, Models and Methods for Engineering Applications, John Wiley & Sons, New York, 1984.
14. Kaimal, J.C., et al., "Spectral Characteristics of Surface Layer Turbulence," Quart. J. Royal Met. Soc., Vol. 98, 1979.
15. Davenport, A.G., "The Spectrum of Horizontal Gustiness Near the Ground in High Winds," Quart. J. Royal Met. Soc., Vol. 87, 1961, pp. 194-211.
16. Madsen, P.H., "Wind Turbulence Loading on Horizontal-Axis Wind Turbines," Draft, Solar Energy Research Institute, Golden, Colorado.
17. Hurty, W.C., and Rubenstein, M.F., Dynamics of Structures, Prentice-Hall, Englewood Cliffs, N.J., 1964.
18. Newland, D.E., An Introduction to Random Vibration and Spectral Analysis, Longman, London, England, 1975.

APPENDIX - Admittance Function Tables

Flapwise bending

μ^*	F_0	F_1	F_2	F_3
0.0100	6.29300	0.00958	0.00029	0.00004
0.0126	6.28200	0.01438	0.00053	0.00008
0.0159	6.26600	0.02136	0.00095	0.00015
0.0200	6.24200	0.03133	0.00168	0.00029
0.0251	6.20900	0.04531	0.00290	0.00053
0.0316	6.16200	0.06452	0.00488	0.00096
0.0398	6.09600	0.09032	0.00800	0.00170
0.0501	6.00700	0.12420	0.01275	0.00292
0.0631	5.88900	0.16750	0.01976	0.00486
0.0794	5.73400	0.22130	0.02976	0.00785
0.1000	5.53500	0.28650	0.04357	0.01228
0.1259	5.28800	0.36270	0.06201	0.01859
0.1585	4.98700	0.44870	0.08589	0.02731
0.1995	4.62900	0.54150	0.11580	0.03892
0.2512	4.21700	0.63620	0.15200	0.05392
0.3162	3.75600	0.72540	0.19420	0.07268
0.3981	3.26100	0.80010	0.24080	0.09532
0.5012	2.75000	0.84990	0.28900	0.12150
0.6310	2.24700	0.86550	0.33430	0.15020
0.7943	1.77800	0.84100	0.37040	0.17920
1.0000	1.36300	0.77660	0.39070	0.20510
1.2590	1.01700	0.68000	0.38980	0.22350
1.5850	0.74170	0.56450	0.36610	0.23020
1.9950	0.53170	0.44580	0.32290	0.22260
2.5120	0.37600	0.33700	0.26780	0.20130
3.1620	0.26280	0.24580	0.21010	0.17040
3.9810	0.18170	0.17460	0.15740	0.13590
5.0120	0.1247	0.12170	0.11390	0.10320
6.3100	0.08539	0.08421	0.08084	0.07587
7.9430	0.05627	0.05604	0.05531	0.05397
10.0000	0.03603	0.03599	0.03585	0.03559
12.5900	0.02284	0.02283	0.02281	0.02276
15.8500	0.01443	0.01443	0.01442	0.01442
19.9500	0.00911	0.00911	0.00911	0.00911
25.1200	0.00575	0.00575	0.00575	0.00575
31.6200	0.00363	0.00363	0.00363	0.00363
39.8100	0.00229	0.00229	0.00229	0.00229
50.1200	0.00144	0.00144	0.00144	0.00144
63.1000	0.00091	0.00091	0.00091	0.00091
79.4300	0.00057	0.00057	0.00057	0.00057
100.0000	0.00036	0.00036	0.00036	0.00036

Edgewise bending

μ^*	F_0	F_1	F_2	F_3
0.0100	6.27400	0.00707	0.00019	0.00003
0.0126	6.26500	0.01066	0.00035	0.00005
0.0159	6.25200	0.01589	0.00063	0.00010
0.0200	6.23300	0.02342	0.00112	0.00018
0.0251	6.20600	0.03404	0.00194	0.00034
0.0316	6.16700	0.04874	0.00329	0.00061
0.0398	6.11200	0.06866	0.00544	0.00109
0.0501	6.03700	0.09502	0.00873	0.00188
0.0631	5.93600	0.12910	0.01364	0.00315
0.0794	5.80200	0.17180	0.02070	0.00512
0.1000	5.62900	0.22410	0.03054	0.00806
0.1259	5.41100	0.28610	0.04381	0.01230
0.1585	5.14000	0.35690	0.06115	0.01820
0.1995	4.81500	0.43470	0.08307	0.02613
0.2512	4.43200	0.51580	0.10990	0.03644
0.3162	3.99700	0.59470	0.14140	0.04945
0.3981	3.51900	0.66420	0.17690	0.06529
0.5012	3.01200	0.71550	0.21440	0.08382
0.6310	2.49800	0.74000	0.25070	0.10440
0.7943	2.00200	0.73140	0.28130	0.12570
1.0000	1.54700	0.68750	0.30110	0.14550
1.2590	1.15400	0.61230	0.30540	0.16070
1.5850	0.83250	0.51580	0.29190	0.16800
1.9950	0.58330	0.41130	0.26180	0.16520
2.5120	0.39920	0.31180	0.22040	0.15200
3.1620	0.26710	0.22640	0.17490	0.13090
3.9810	0.17470	0.15820	0.13170	0.10590
5.0120	0.11260	0.10610	0.09502	0.08122
6.3100	0.07203	0.06946	0.06507	0.05937
7.9430	0.04584	0.04483	0.04310	0.04085
10.0000	0.02908	0.02868	0.02801	0.02712
12.5900	0.01841	0.01826	0.01799	0.01765
15.8500	0.01164	0.01158	0.01148	0.01135
19.9500	0.00735	0.00733	0.00730	0.00725
25.1200	0.00464	0.00464	0.00462	0.00461
31.6200	0.00293	0.00293	0.00293	0.00292
39.8100	0.00185	0.00185	0.00185	0.00185
50.1200	0.00117	0.00117	0.00117	0.00117
63.1000	0.00074	0.00074	0.00074	0.00074
79.4300	0.00046	0.00046	0.00046	0.00046
100.0000	0.00029	0.00029	0.00029	0.00029